

Evidence of liquid dependent ice nucleation in high-latitude stratiform clouds from surface remote sensors

G. de Boer,¹ H. Morrison,² M. D. Shupe,³ and R. Hildner⁴

Received 29 October 2010; revised 24 November 2010; accepted 5 December 2010; published 6 January 2011.

[1] Ground-based lidar, radar and microwave radiometer observations at Eureka, Canada, Barrow, Alaska and over the western Arctic Ocean measure physical characteristics and morphology of stratiform clouds. Despite transition of a cold atmosphere (-15 C) through ice supersaturated conditions, ice is not observed until soon after a liquid layer. Several cases illustrating this phenomenon are presented in addition to long-term observations from three measurement sites characterizing cloud phase frequency. This analysis demonstrates that clouds composed entirely of ice occur less frequently than liquid-topped mixed-phase clouds at temperatures warmer than -25 to -30 C . These results indicate ice formation generally occurs in conjunction with liquid at these temperatures, and suggest the importance of liquid-dependent ice nucleation mechanisms. **Citation:** de Boer, G., H. Morrison, M. D. Shupe, and R. Hildner (2011), Evidence of liquid dependent ice nucleation in high-latitude stratiform clouds from surface remote sensors, *Geophys. Res. Lett.*, 38, L01803, doi:10.1029/2010GL046016.

1. Introduction

[2] Arctic climate is changing at a rate exceeding that of other regions [Symon *et al.*, 2005]. Quantitative predictions of high-latitude changes, and impacts on future climate, rely on sophisticated climate models. Despite expanded efforts, models still struggle to accurately portray cloud processes, resulting in surface and atmospheric radiative budget errors [e.g., Klein *et al.*, 2009]. Of observed high-latitude clouds, mixed-phase stratiform (MPS) layers are among the most radiatively influential [e.g., Shupe *et al.*, 2006].

[3] Modeling studies [e.g., Harrington and Olsson, 2001] show MPS lifetime depends strongly on ice concentration due to efficiency of the Bergeron-Findeissen process [Pruppacher and Klett, 1997]. Therefore, understanding ice nucleation in these layers is imperative. Heterogeneous ice formation at temperatures (T) $> -40\text{ C}$ may occur via several primary modes, namely deposition, condensation, immersion and contact freezing. In deposition freezing, ice-supersaturated conditions result in deposition of water

vapor onto ice forming nuclei (IN), forming ice crystals. Condensation freezing is similar, except aerosol particles (hereafter particles) involved are less efficient IN, possibly containing both soluble and insoluble mass. These mixed particles are observed at high-latitudes, often as dust or soot and sulfates or organics [e.g., Bigg and Leck, 2001]. Soluble mass on these particles requires an environment approaching water saturation to undergo sufficient wetting to nucleate ice. Immersion freezing is comparable to condensation freezing, except droplets grow to super-critical sizes (transitioning from haze to cloud droplets) before freezing. Finally, contact nucleation involves collision of existing water droplets with IN.

[4] Several recent theories on Arctic MPS ice formation have been presented, including immersion nucleation [de Boer *et al.*, 2009b], evaporation ice nucleation [Fridlind *et al.*, 2007], and contact nucleation [Morrison *et al.*, 2005]. Additionally, Prenni *et al.* [2009] presented in-situ observations indicating immersion or condensation nucleation are important mechanisms within these clouds. Because MPS are observed in T between -40 and 0 C [Shupe *et al.*, 2006; de Boer *et al.*, 2009a], no heterogeneous nucleation mechanism can be ruled out due to conditions alone. However, observations demonstrate patterns in timing of liquid and ice formation, providing clues toward understanding ice nucleation. We present observations demonstrating instances when ice, despite having a lower saturation vapor pressure than liquid, is not formed without presence of liquid. Statistics of observed cloud phase are provided to generalize these findings.

2. Instruments

[5] Observations come from a combination of Arctic surface-based remote sensors. Included are data from a 35 GHz Millimeter Cloud Radar (MMCR) [Moran *et al.*, 1998] and microwave radiometer (MWR) at the US Department of Energy (DOE) Atmospheric Radiation Measurement (ARM) facility in Barrow, Alaska, the Study of Environmental Arctic Change (SEARCH) site in Eureka, Canada and the Beaufort Sea Surface Heat Budget of the Arctic (SHEBA) [Uttal *et al.*, 2002] campaign. Additionally, Wisconsin Arctic High Spectral Resolution Lidar (AHSRL Eureka and some Barrow) [Eloranta, 2005], micropulse lidar (MPL, Barrow) and Depolarization and Backscatter Unattended Lidar (DABUL, SHEBA) [Grund and Sandberg 1996] measurements were used. Observation periods include 12/06/07-10/01/98 (SHEBA all times with active MWR), 02/04-02/06 (Barrow) and 08/05-10/09 (Eureka). Because the MMCR and lidars operate at different wavelengths, their measurements respond differently to various hydrometeors. In MPS, lidars are more sensitive

¹Environmental Energy Technologies Division, Lawrence Berkeley National Laboratory, Berkeley, California, USA.

²National Center for Atmospheric Research, Boulder, Colorado, USA.

³Cooperative Institute for Research in Environmental Sciences, University of Colorado at Boulder, PSD, ESRL, NOAA, Boulder, Colorado, USA.

⁴Department of Atmospheric and Oceanic Science, University of Wisconsin-Madison, Madison, Wisconsin, USA.

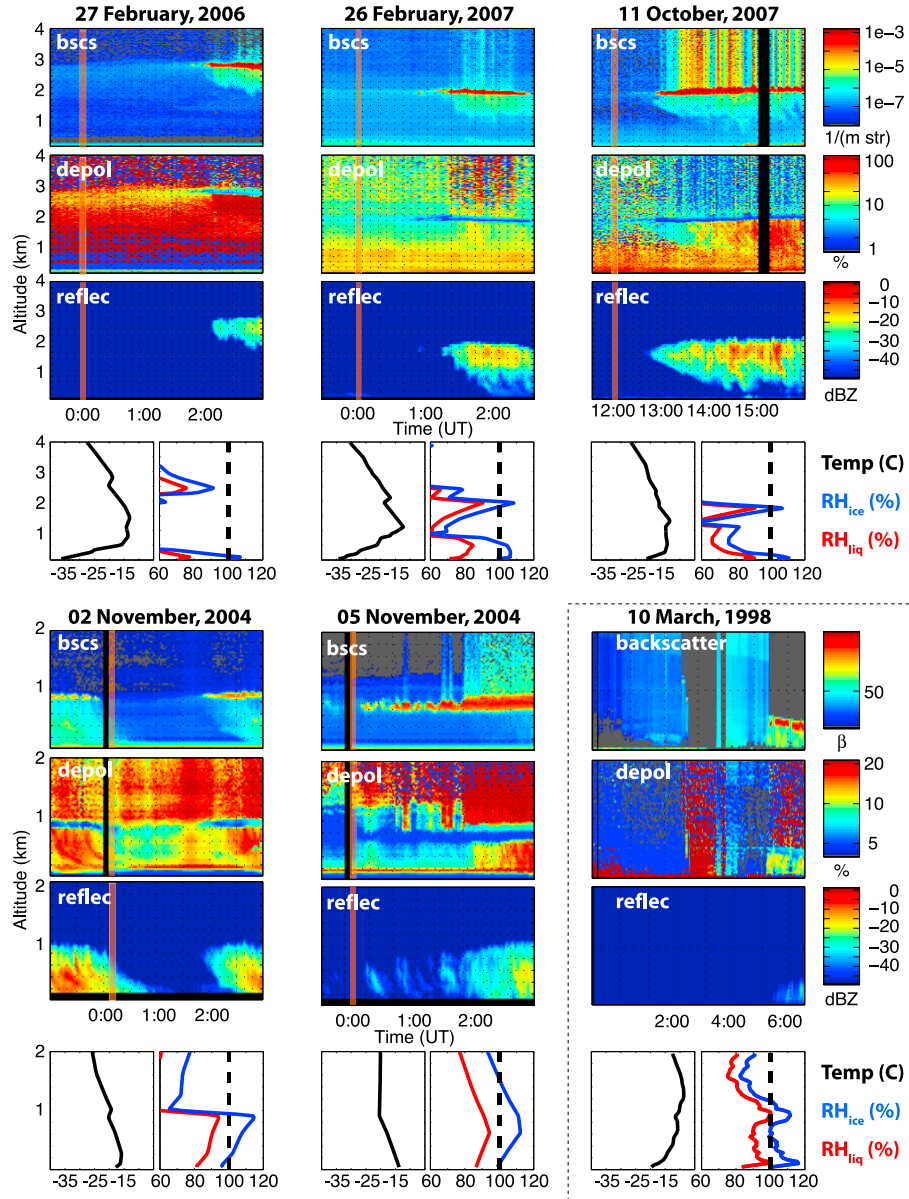


Figure 1. Six examples of MPS cloud appearance at various Arctic sites. From top to bottom, the figures include lidar backscatter cross-section, lidar depolarization ratio, radar reflectivity and thermodynamic profiles. The orange bars in the backscatter, depolarization and reflectivity plots indicate the radiosonde launch time. The upper three colorbars are for all but the bottom righthand plots (separated by dotted lines), which has its own colorbars.

to the large combined cross-sectional area from high concentrations of liquid droplets [McFarquhar *et al.*, 2007], while the MMCR signal is dominated by fewer but larger ice crystals. Lidar depolarization measurements from the AHSRL and DABUL help distinguish between non-depolarizing particles (e.g., spheres) and depolarizing particles. In addition to remotely sensed measurements, T and relative humidity (RH) are from radiosondes (sondes). These sondes may exhibit dry biases at low T [e.g., Miloshevich *et al.*, 2009]. However, given the range of sonde models used no corrections are applied to presented measurements, in part to avoid confusion about their influence on RH profiles. The (possibly dry-biased) profiles presented provide

adequate evidence that the atmosphere approached or exceeded ice saturation in clear-sky conditions.

3. Methods and Results

[6] Qualitative and statistical evaluations of ice presence in MPS clouds are presented. Six cases (02/27/06, 02/26/07 and 10/11/07 – Eureka; 11/02/04 and 11/05/04 – Barrow; and 03/10/98 – SHEBA) are examples of a more broadly observed phenomenon. These cases illustrate MPS at multiple locations and times of year. Provided in Figure 1 are lidar backscatter cross-section (or backscatter for DABUL) (β'), lidar depolarization ratio (δ), radar reflectivity (Z_{mmcr}) and T and RH profiles. T and RH are from sondes launched

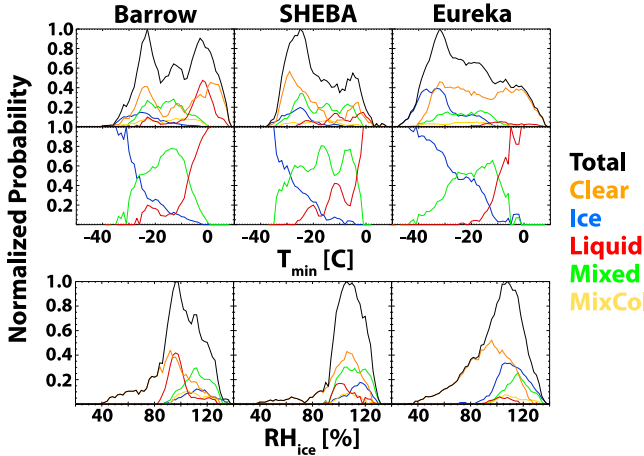


Figure 2. The normalized probability of occurrence of clouds of different phases under a range of T and RH with respect to ice for the three observational sites. The vertical axis is normalized (top and bottom) to the highest recorded occurrence in plots including the total amount, and (middle) to the total cases included.

at the time indicated by orange bars. For 10 March, DABUL was not operating at 00Z, but MMCR reflectivity showed no sign of clouds or precipitation.

[7] All cases illustrate similar patterns in appearance and evolution of an MPS layer. Low β' is indicative of clear air. This layer is exposed to cold ($-25^{\circ}C \leq T \leq -10^{\circ}C$) and humid ($RH_{ice} \geq 100\%$) conditions at the time of sonde measurements. When approaching liquid saturation, aerosol particles swell to form haze, increasing β' and decreasing δ . Haze is distinguishable from small ice through lidar δ , with observed decreases in δ due to the sphericity of haze droplets. With cloud droplet formation, there is a dramatic increase in β' and soon after the cloud develops, increased in- and below-cloud Z_{mmcr} and below-cloud δ indicate presence of ice. For cloud droplet formation RH_{liq} must reach 100%, requiring atmospheric cooling and/or moistening from the sonde profiles, both favorable for ice formation and growth. Despite this, no ice is detected prior to the appearance of liquid. Additionally, 11/02/04 illustrates a lack of ice after liquid disappears, despite RH_{ice} between 100 and 115%. It should be noted that while among the most sensitive radars, the MMCR cannot detect newly nucleated ice that has not undergone growth. Assuming small spherical ice at concentrations of 1 L^{-1} , the minimum detectable reflectivity ($\approx 55\text{ dBZ}$ at low altitudes) would occur when crystals grow to roughly $50\text{ }\mu\text{m}$. Under typical conditions from presented profiles ($T = -20^{\circ}C$ and $RH_{ice} = 110\%$), a capacitance growth model predicts ice with a $5\text{ }\mu\text{m}$ radius to grow to this size in roughly 790 seconds. At RH_{ice} closer to liquid saturation (roughly 122% for $T = -20^{\circ}C$), this growth would occur even faster. Assuming a 10 cm s^{-1} average fall speed, this crystal would fall 79 meters during that time, keeping it within ice-saturated conditions (ranging between 200 and 1600 m for presented cases).

[8] To generalize these findings, hydrometeor phase under varying T and RH is analyzed. Remotely sensed data are used to derive cloud phase using a fixed-threshold, multi-sensor classification. This classification and thresh-

olds used are presented by Shupe [2007]. Profiles are limited to 20 minutes surrounding sonde launches and conditions with no hydrometeors above four kilometers. Minimum T (T_{\min}) reported is either the lowest in-cloud T (when cloudy) or lowest T below four kilometers altitude (when clear), while reported RH with respect to ice (RH_{ice}) represents the highest value below four kilometers. The “Mixed” category represents the structure of interest (liquid topped MPS), while “MixCol” represents ice-topped clouds with embedded mixed-phase layers.

[9] Figure 2 illustrates normalized probabilities of analyzed phase occurrence with respect to T_{\min} (Figures 2, top and 2, middle) and RH_{ice} (Figure 2, bottom). Both distributions for all classifications (Figure 2, top), and for ice only, liquid only and “mixed” (Figure 2, middle) are shown. Barrow and SHEBA have few cases where $T_{\min} < -40^{\circ}C$ below 4 km. At all locations, MPS are the most common cloud type roughly when $-10^{\circ}C < T_{\min} < -25^{\circ}C$. Not surprisingly, liquid clouds are more common than ice containing ones at $T_{\min} > -10^{\circ}C$, and ice clouds are more common than liquid-containing ones when $T_{\min} < -30^{\circ}C$. Interestingly, for Barrow and SHEBA MPS are more common than ice clouds at all RH_{ice} . This is not true at Eureka, due mainly to a large number of ice cloud cases at low T_{\min} . These statistics indicate that over a range of ice-friendly conditions ($-25^{\circ}C < T_{\min} < -10^{\circ}C$, $RH_{ice} \geq 100\%$) MPS are dominant.

[10] Figure 3 shows scatter plots of phase in T_{\min} - RH_{ice} space. Liquid and MPS cases roughly fall in line with the Clausius-Clapeyron relation at water saturation (dashed grey line). Observations falling above this line are likely a result of T_{\min} and RH_{ice} definitions used and radiosonde errors. Similarly, presence of ice and MPS at $RH_{ice} < 100\%$ is likely explained by radiosonde dry-biases discussed previously or radiosonde drift with altitude. All locations show similar distributions of MPS at $-25^{\circ}C < T_{\min} < -10^{\circ}C$. At warmer T_{\min} , Barrow appears to have more liquid clouds

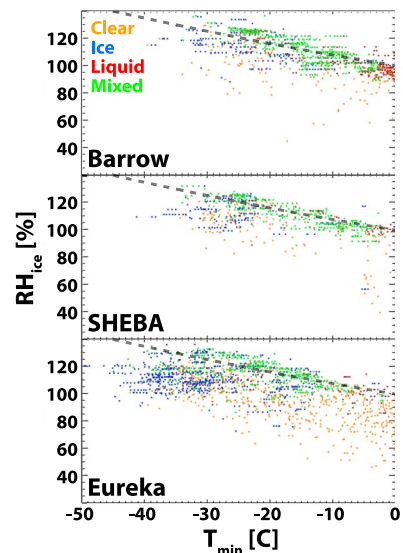


Figure 3. A scatterplot demonstrating the T and RH conditions of all cases observed in each of the three locations. Phase is separated by different colors as indicated, and the Clausius-Clapeyron curves for liquid saturation are shown by the grey dashed lines.

than SHEBA or Eureka, while Eureka has more ice clouds at colder T_{\min} . Eureka ice clouds mainly occur when $T_{\min} < -25^{\circ}\text{C}$. Eureka has more clear cases, occurring at all T at low RH. With few exceptions, ice is present by itself only in situations where $T_{\min} < -25^{\circ}\text{C}$ and $100\% \leq \text{RH}_{ice} < \text{liquid saturation}$. Under these conditions, little liquid is observed, likely due to consumption of water vapor by ice growth.

4. Discussion and Summary

[11] These observations demonstrate several interesting phenomena. First, as observed by Kanji and Abbott [2006], aerosol layers detected at -20°C under ice-supersaturated conditions do not readily form ice via the deposition mode. This may be due to aerosol chemistry, though this can not be proven with the sensors employed. This pattern appears robust over a range of seasons and locations. Appearance of ice once liquid is established suggests liquid-related ice nucleation. While responsible pathways can not be determined from these measurements alone, it supports liquid-dependent mechanisms such as contact nucleation, immersion freezing, or evaporation freezing, and falls in line with previous in-situ analyses [e.g., Prenni *et al.*, 2009; Rangno and Hobbs, 2001] and discussions on super-cooled liquid [e.g., Rauber and Tokay, 1991]. Condensation and deposition freezing do not appear to readily occur prior to cloud droplet nucleation, since haze layers are observed with no evidence of ice formation and growth. While utilized measurements are incapable of proving inactivity of condensation and deposition freezing after liquid forms, it seems unlikely that these mechanisms would be initiated and dominate right at liquid saturation.

[12] Long-term statistics presented, while not directly providing phase order of appearance, supply evidence that ice clouds occur far less frequently than MPS at $T > -25^{\circ}\text{C}$. We speculate that ice-first morphology via deposition or condensation freezing regimes would result in increased ice-only observations, due in part to an ice-induced sink of atmospheric water vapor limiting cloud formation. A lack of ice-only cases together with individual examples of morphology suggests that liquid droplets may be an important driver for ice nucleation at $T > -25^{\circ}\text{C}$. This is consistent with findings of Ansmann *et al.* [2009] who showed a strong relationship between initiation of ice and presence of liquid in tropical altocumulus, Hobbs and Rangno [1985] demonstrating links between presence of liquid droplets and increased ice amounts from analysis of in-situ measurements, Cooper and Vali [1981] describing limited effectiveness of deposition freezing in continental wave clouds and Ohtake *et al.* [1982] who assessed ice forming in the lower Arctic atmosphere to mainly result from droplet freezing. The idea of liquid-dependent ice nucleation also supports work by Rangno and Hobbs [2001] who demonstrated a relationship between ice concentration and droplet threshold diameter for Arctic clouds. Generalization of these findings to global scales will require further observational analysis, including a review of satellite data.

[13] Finally, these observations have implications on simulation of ice nucleation in models of all scales. Many microphysical schemes allow nucleation of ice below water saturation when $-25^{\circ}\text{C} \leq T \leq 10^{\circ}\text{C}$ [e.g., Lin *et al.*, 1983; Hong *et al.*, 2004; Morrison and Gettelman, 2008]. Observations presented imply that limiting ice nucleation when

$RH_{liq} < 100\%$ and $-25^{\circ}\text{C} \leq T \leq 0^{\circ}\text{C}$ (or conversely increasing ice nucleation at $RH_{liq} = 100\%$) may be prudent, and support improvement of parameterizations of immersion and contact freezing. Additionally, possible impacts of aerosol chemistry makes improved aerosol modules important contributors to realistic microphysical simulation.

[14] **Acknowledgments.** The authors acknowledge E. Eloranta, J. Hedrick, J. Garcia and I. Razenkov for AHSRL data and R. Moritz for advice on SHEBA sonde measurements, as well as DOE, NOAA and SEARCH teams for MMCR data. Information from Eureka weather station personnel was helpful in dataset compilation. Data were also made available by the US DOE ARM program, and the SHEBA team. Finally, we acknowledge funding from the National Aeronautics and Space Administration (NASA: NNX07AQ81G) and US DOE (U.S. DOE: ER64187-1027586-0011923 and DE-FG02-05ER63965). NCAR is sponsored by the National Science Foundation. LBNL is managed by the University of California under U.S. DOE grant DE-AC02-05CH11231.

References

- Ansmann, A., M. Tesche, P. Seifert, D. Althausen, R. Engelmann, J. Frunke, U. Wandinger, I. Mattis, and D. Müller (2009), Evolution of the ice phase in tropical altocumulus: SAMUM lidar observations over Cape Verde, *J. Geophys. Res.*, 114, D17208, doi:10.1029/2008JD011659.
- Bigg, E. K., and C. Leck (2001), Cloud-active particles over the central Arctic Ocean, *J. Geophys. Res.*, 106, 32,155–32,166.
- Cooper, W. A., and G. Vali (1981), The origin of ice in mountain cap clouds, *J. Atmos. Sci.*, 38, 1244–1259.
- de Boer, G., E. Eloranta, and M. Shupe (2009a), Arctic mixed-phase stratiform cloud properties from multiple years of surface-based measurements at two high-latitude locations, *J. Atmos. Sci.*, 66(9), 2874–2887, doi:10.1175/2009JAS3029.1.
- de Boer, G., T. Hashino, and G. J. Tripoli (2009b), A theory for ice nucleation through immersion freezing in mixed-phase stratiform clouds, *Atmos. Res.*, 96, 315–324, doi:10.1016/j.atmosres.2009.09.012.
- Eloranta, E. (2005), High spectral resolution lidar, in *Lidar: Range-Resolved Optical Remote Sensing of the Atmosphere*, edited by K. Weitkamp, pp. 143–163, Springer, New York.
- Fridlind, A. M., A. S. Ackerman, G. McFarquhar, G. Zhang, M. R. Poellot, P. J. DeMott, A. J. Prenni, and A. J. Heymsfield (2007), Ice properties of single-layer stratocumulus during the Mixed-Phase Arctic Cloud Experiment: 2. Model results, *J. Geophys. Res.*, 112, D24202, doi:10.1029/2007JD008646.
- Grund, C., and S. Sandberg (1996), Depolarization and backscatter lidar for unattended operation, in *Proceedings of the 18th International Laser Radar Conference*, pp. 3–6, Springer, Berlin.
- Harrington, J. Y., and P. Q. Olsson (2001), On the potential influence of ice nuclei on surface-forced marine stratocumulus cloud dynamics, *J. Geophys. Res.*, 106, 27,473–27,484.
- Hobbs, P., and A. Rangno (1985), Ice particle concentrations in clouds, *J. Atmos. Sci.*, 42(23), 2523–2549.
- Hong, S.-Y., J. Dudhia, and S.-H. Chen (2004), A revised approach to ice microphysical processes for the bulk parameterization of clouds and precipitation, *Mon. Weather Rev.*, 132, 103–120.
- Kanji, Z. A., and J. P. D. Abbott (2006), Laboratory studies of ice formation via deposition mode nucleation onto mineral dust and n-hexane soot samples, *J. Geophys. Res.*, 111, D16204, doi:10.1029/2005JD006766.
- Klein, S., et al. (2009), Intercomparison of model simulations of mixed-phase clouds observed during the ARM Mixed-Phase Arctic Cloud Experiment. Part I: Single layer cloud, *Q. J. R. Meteorol. Soc.*, 135, 979–1002.
- Lin, Y.-L., R. Farley, and H. Orville (1983), Bulk parameterization of the snow field in a cloud model, *J. Appl. Meteorol.*, 22, 1065–1089.
- McFarquhar, G. M., G. Zhang, M. R. Poellot, G. L. Kok, R. McCoy, T. Tooman, A. Fridlind, and A. J. Heymsfield (2007), Ice properties of single-layer stratocumulus during the Mixed-Phase Arctic Cloud Experiment: 1. Observations, *J. Geophys. Res.*, 112, D24201, doi:10.1029/2007JD008633.
- Miloshevich, L. M., H. Vömel, D. N. Whiteman, and T. Leblanc (2009), Accuracy assessment and correction of Vaisala RS92 radiosonde water vapor measurements, *J. Geophys. Res.*, 114, D11305, doi:10.1029/2008JD011565.
- Moran, K., B. Martner, M. Post, R. Kropfli, D. Welsch, and K. Widener (1998), An unattended cloud-profiling radar for use in climate research, *Bull. Am. Meteorol. Soc.*, 79, 443–455.

- Morrison, H., and A. Gettelman (2008), A new two-moment bulk stratiform cloud microphysics scheme in the Community Atmosphere Model (CAM3). Part I: Description and numerical tests, *J. Clim.*, **21**, 3642–3659.
- Morrison, H., M. D. Shupe, J. O. Pinto, and J. A. Curry (2005), Possible roles of ice nucleation mode and ice nuclei depletion in the extended life-time of Arctic mixed-phase clouds, *Geophys. Res. Lett.*, **32**, L18801, doi:10.1029/2005GL023614.
- Ohtake, T., K. Jayaweera, and K.-I. Sakurai (1982), Observation of ice crystal formation in lower Arctic atmosphere, *J. Atmos. Sci.*, **39**, 2898–2904.
- Prenni, A., P. De Mott, D. Rogers, S. Kreidenweis, G. McFarquhar, G. Zhang, and M. Poellot (2009), Ice nuclei characteristics from m-pace and their relation to ice formation in clouds, *Tellus, Ser. B*, **61**, 436–448.
- Pruppacher, H., and J. Klett (1997), *Microphysics of Clouds and Precipitation*, 2nd ed., Kluwer Acad., Boston, Mass.
- Rangno, A. L., and P. V. Hobbs (2001), Ice particles in stratiform clouds in the Arctic and possible mechanisms for the production of high ice concentrations, *J. Geophys. Res.*, **106**, 15,065–15,075.
- Rauber, R., and A. Tokay (1991), An explanation for the existence of supercooled water at the top of cold clouds, *J. Atmos. Sci.*, **48**, 1005–1023.
- Shupe, M. D. (2007), A ground-based multisensor cloud phase classifier, *Geophys. Res. Lett.*, **34**, L22809, doi:10.1029/2007GL031008.
- Shupe, M., S. Matrosov, and T. Uttal (2006), Arctic mixed-phase cloud properties derived from surface-based sensors at SHEBA, *J. Atmos. Sci.*, **63**, 697–711.
- Symon, C., L. Arris, and B. Heal (Eds.) (2005), *Arctic Climate Impact Assessment*, Cambridge Univ. Press, Cambridge, U. K.
- Uttal, T., et al. (2002), Surface heat budget of the Arctic Ocean, *Bull. Am. Meteorol. Soc.*, **83**, 255–275.
-
- G. de Boer, Environmental Energy Technologies Division, Lawrence Berkeley National Laboratory, MS90KR107, 1 Cyclotron Rd., Berkeley, CA 94720, USA. (gdeboer@lbl.gov)
- R. Hildner, Department of Atmospheric and Oceanic Sciences, University of Wisconsin-Madison, 1225 West Dayton St., Madison, WI 53562, USA.
- H. Morrison, National Center for Atmospheric Research, PO Box 3000, Boulder, CO 80307, USA.
- M. D. Shupe, Cooperative Institute for Research in Environmental Sciences, University of Colorado at Boulder, PSD, ESRL, NOAA, 325 Broadway, Boulder, CO 80305, USA.